Analysis of the phase transition sequence of the elpasolite (ordered perovskite) Pb_2MgTeO_6

1997 J. Phys.: Condens. Matter 9 10531

(http://iopscience.iop.org/0953-8984/9/47/020)

J. Phys.: Condens. Matter **9** (1997) 10531–10544. Printed in the UK PII: S0953-8984(97)84532-8

Analysis of the phase transition sequence of the elpasolite (ordered perovskite) Pb_2MgTeO_6

G Baldinozzi†, Ph Sciau† and A Bulou‡

† Laboratoire de Chimie Physique du Solide, URA CNRS 453, Ecole Centrale Paris, F-92295 Châtenay-Malabry Cédex, France

‡ Laboratoire de Physique de l'Etat Condensé, CNRS UPRES-A 6087, Université du Maine, F-72085 Le Mans Cédex 9, France

Received 6 June 1997, in final form 5 September 1997

Abstract. The elpasolite compound lead magnesium tellurate Pb_2MgTeO_6 undergoes a structural phase transition at about 194 K. This phase transition has been characterized by calorimetry, by dielectric permittivity measurements and by Raman spectroscopy. The main features of the Raman spectra, collected between 35 K and room temperature, are consistent with group-theoretical predictions, though the onset of the incommensurate superstructure gives rise to a very complex splitting of the cubic lines. From the comparison between these results and the structures, it is concluded that the phase transition is only weakly first order and has a mainly displacive character. The thermal evolution of the Raman spectra and of the dielectric permittivity support the existence of an additional phase transition at about 142 K.

1. Introduction

The prototype structure of perovskite compounds (ABO_3) consists of a regular repetition of oxygen-sharing octahedra BO_6 along the three $\langle 100 \rangle$ directions. If the cation B, situated at the centre of the octahedron, is replaced by two different species of cation, namely B′ and B″, a complex perovskite structure is obtained. Depending upon the stoichiometry, charge and cationic size differences, the structure may be ordered or not. The prototype structure of the materials $A_2B'B''O_6$ exhibiting cationic ordering along $\langle 111 \rangle$ directions is called elpasolite. This structure is cubic $Fm\bar{3}m$, as doubling of the simple perovskite lattice parameter occurs.

Powder samples of Pb_2MgTeO_6 were first synthesized and characterized by Bayer (1963). Up to now this compound has not been obtained as single crystal. The room temperature phase of the highly ordered perovskite-like Pb_2MgTeO_6 has the elpasolite structure. Dielectric measurements performed by Politova and Venevtsev (1973) show a small anomaly in $\epsilon'(T)$ and $\epsilon''(T)$ at about 190 K. In fact, this compound undergoes a weakly first-order structural phase transition at about 194 K (Baldinozzi *et al* 1994) as shown by x-ray diffraction. This transition is ferroelastic and it separates the high-temperature cubic phase ($Fm\bar{3}m$) from the lower-temperature rhombohedral one. The low-temperature phase is incommensurate with a modulation vector ($\delta\delta\delta$) where δ is close to 0.107 at 8 K.

The onset of an incommensurate phase in complex perovskites seems to be a quite unusual phenomenon. Only three other examples of modulated phases in complex perovskites have been observed: the monoclinic phases of Pb_2CoWO_6 (Tamura 1978) and of Pb_2CdWO_6 (Sciau and Grebille 1994), and possibly the trigonal phase of $Pb(ScTa)_{1/2}O_3$

0953-8984/97/4710531+14$19.50

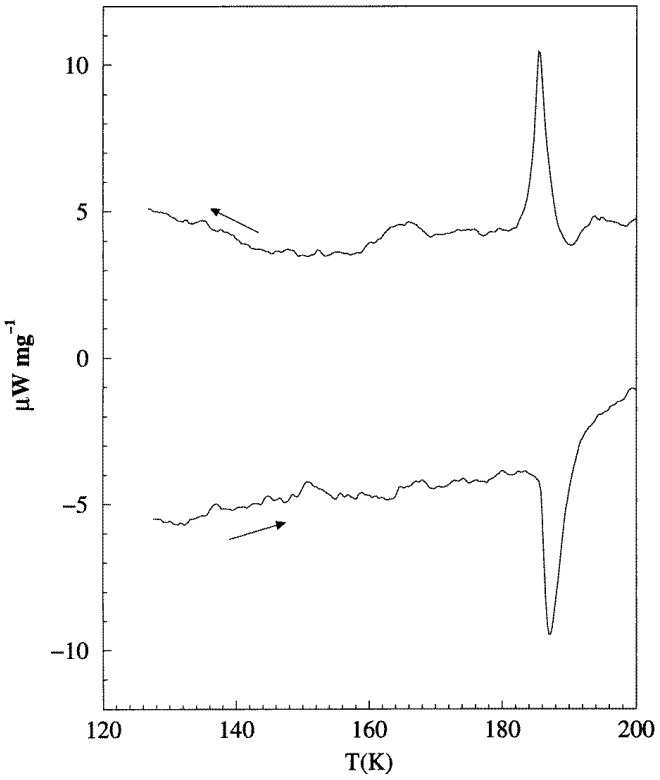

Figure 1. The DSC curve of the phase transition on heating and cooling (temperature rate: 3 K min^{-1}).

(Randall *et al* 1989). The incommensurate phase of Pb_2MgTeO_6 is very unusual because of the large range of existence: no lock-in occurs at least down to 8 K.

The present paper is devoted to an experimental study of the phase transition by calorimetry, dielectric permittivity measurements and Raman scattering experiments in order to establish precisely the mechanism of the transition. The mode analysis shows that the atomic displacements can be described as sums of atomic displacements associated with the wavevector $\boldsymbol{q}_{inc} = \delta\boldsymbol{a}^\star + \delta\boldsymbol{b}^\star + \delta\boldsymbol{c}^\star$ where δ is close to $\frac{1}{9}$. The transition mechanism seems to be essentially of displacive nature.

2. Synthesis

Powdered samples of Pb_2MgTeO_6 have been obtained by J Moret, starting from stoichiometric amounts of high-purity PbO, TeO_2 and MgO as described in a previous paper (Baldinozzi *et al* 1994).

The powders of Pb_2MgTeO_6 obtained were well crystallized; the examination of the sample by x-ray diffraction indicated good quality of the synthesis. Some very weak additional peaks were observed; they may be attributed, by comparison to lower-quality syntheses, to Pb_3TeO_6 and $PbTeO_3$ impurities.

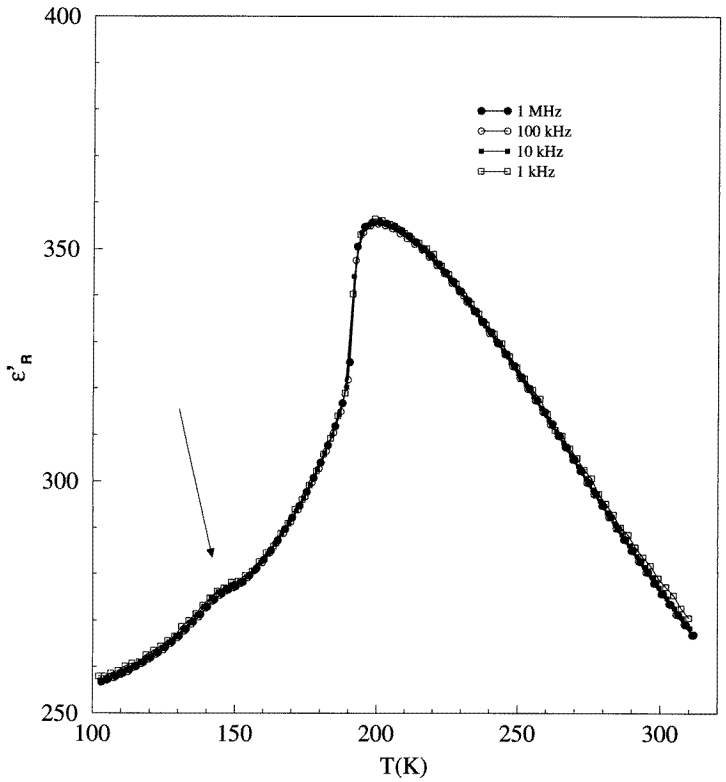

Figure 2. The dielectric permittivity versus T at different frequencies. No shift of the peak maximum associated with the phase transition versus frequency is observed.

3. Results

3.1. Calorimetry

Differential scanning calorimetry measurements were performed using a Seiko DSC 220C microcalorimeter. The sample (300 mg) was loaded in an aluminium crucible, and α-Al_2O_3 was taken as the reference. Scans on heating and on cooling were performed in the range 123–300 K at a temperature rate of 3–5 K min^{-1}.

As we have already discussed in a previous paper (Baldinozzi *et al* 1994), the onset of the incommensurate phase transition is not accompanied by any significant step discontinuity of the lattice parameters. The analysis of the DSC diagram (figure 1) shows a peak at the phase transition at about 188 K on heating. This temperature is in good agreement with the value (194 ± 2 K) obtained by fitting the intensities of satellite peaks with a critical exponent law. Even though this peak is rather weak, giving a latent heat of 0.3 J g^{-1}, a hysteresis of less than 4 K is observed. Therefore, we can safely affirm that this phase transition is weakly first order.

3.2. Dielectric permittivity

The dielectric permittivity measurements were performed with an impedance analyser, Hewlett–Packard 4192A, at various frequencies between 1 kHz and 1 MHz in the

temperature range 100–330 K on a silver-coated ceramic sample ($\varnothing = 6$ mm, 0.2 mm thick). The thermal stability during the measurements was better than 1 K.

In the paper by Politova and Venevtsev (1973), measurements of the dielectric permittivity were reported, showing a dependence of the maximum of the dielectric permittivity on the frequency. This behaviour, typical of a relaxor material, disagrees with the characteristic of a high degree of order for this material. We have therefore checked this point, performing different series of dielectric constant measurements at different frequencies, both on heating and on cooling. In fact no relaxation is observed, and the maximum of the dielectric permittivity occurs at about 194 K (figure 2). Moreover, ϵ'' is extremely weak and no peak is observed. It is worth noting the existence, at all frequencies (but only on cooling), of a small anomaly affecting ϵ' at about 145 K. This anomaly is possibly related to a modification of the modulation regime in the crystal, and it occurs in correspondence with the saturation of the amplitude of the modulation vector.

The same measurements, performed on the sample submitted to electric fields up to 10 kV cm^{-1}, do not show any significant difference. Therefore, we have supposed the phase transition to be an antiferroelectric one.

3.3. Electron microscopy

As has been discussed in a previous paper (Baldinozzi *et al* 1994), a ferroelastic incommensurately modulated phase transition occurs at 194 K. The symmetry of the low-temperature phase was found to be trigonal. At that time we were not able to propose a space group for this phase.

The electron diffraction patterns, along the $[110]_c$ zone axis at about 100 K, contain extra spots lying at incommensurate positions near the face-centred-cubic lattice spots. In the same paper, it was shown that the modulated phase is mono-incommensurate, and that satellites of all orders can be indexed by a one-dimensional modulation vector $\boldsymbol{q}_{inc} = \delta\boldsymbol{a}^\star + \delta\boldsymbol{b}^\star + \delta\boldsymbol{c}^\star$, $\delta \sim \frac{1}{9}$.

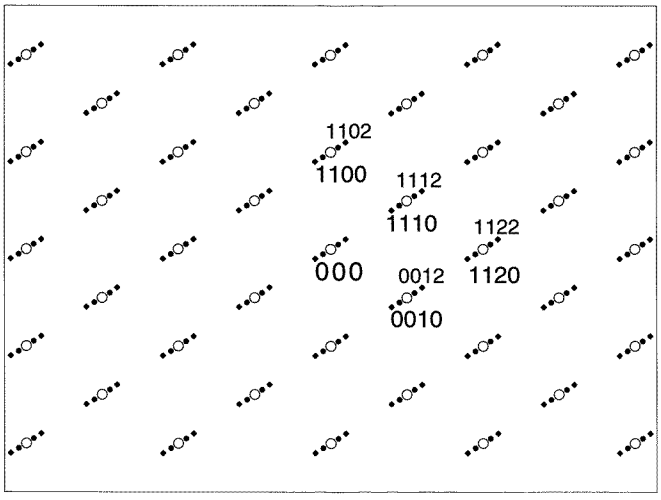

Figure 3. A schematic representation of the diffraction pattern observed along the zone axis $[110]_c$ at about 100 K in a single-domain region. The spots are indexed according to the incommensurate trigonal symmetry.

It should be noticed that our choice of modulation vector $\boldsymbol{q}$ is compatible with the four-dimensional (Wilson 1992) trigonal Bravais class number 22 for mono-incommensurate structures ($\bar{3}mR(00\gamma)$). In the following, the results refer to the rhombohedral setting instead of the hexagonal one, in order to allow us to work with primitive lattices. An electron microscopy plate already published (Baldinozzi *et al* 1994) has also been indexed in this rhombohedral setting; this is shown in figure 3.

The analysis of a large number of electron microscopy plates for the modulated phase allowed us to safely conclude that no systematic extinction affects the satellite spots. As the same characteristic feature is observed for the powder diffraction patterns too, the only acceptable superspace groups compatible with the previous restrictions are $R\bar{3}m(\delta\delta\delta)$, $R\bar{3}(\delta\delta\delta)$, and the corresponding non-centrosymmetrical space groups.

Table 1. Atomic positions in the space group $Fm\bar{3}m$.

Atom	Site symmetry	x	y	z
Te	O_h	0	0	0
Mg	O_h	0	0	$\frac{1}{2}$
Pb_1	T_d	$\frac{1}{4}$	$\frac{1}{4}$	$\frac{1}{4}$
Pb_2	T_d	$\frac{1}{4}$	$\frac{1}{4}$	$\frac{3}{4}$
O_1	C_{4v}	0	0	ξ
O_2	C_{4v}	0	0	$1-\xi$
O_3	C_{4v}	ξ	0	0
O_4	C_{4v}	0	ξ	0
O_5	C_{4v}	$\frac{1}{2}-\xi$	0	$\frac{1}{2}$
O_6	C_{4v}	0	$\frac{1}{2}-\xi$	$\frac{1}{2}$

3.4. Symmetry analysis

In the following, the phase transition mechanism is studied in the framework of the analysis of the symmetry of the modes at two points of the Brillouin zone: at the centre ($\boldsymbol{k}_0 = \boldsymbol{0}$) and at the point where a mode is expected to condense ($\boldsymbol{q}_{inc} = \delta\boldsymbol{a}^\star + \delta\boldsymbol{b}^\star + \delta\boldsymbol{c}^\star$, $\delta \sim \pm\frac{1}{9}$). For this purpose, it is necessary to determine the decomposition of the high-temperature mode symmetries into the irreducible representations at these points. Knowledge of the relationships between the symmetry elements of the two phases allows one to establish the relationships between the phases, and to look for the modes which can condense giving rise to the low-temperature phase. The positions of the atoms in the cubic phase are reported in table 1.

3.4.1. Cubic phase symmetry. The normal modes of vibration of the cubic phase of elpasolite compounds at the Brillouin zone centre ($\boldsymbol{k}_0 = \boldsymbol{0}$) can be classified according to the following irreducible representations:

$$\Gamma(\boldsymbol{k}_0) = A_{1g} \oplus E_g \oplus T_{1g} \oplus 2T_{2g} \oplus 5T_{1u} \oplus T_{2u}.$$

The A_{1g} mode is the totally symmetrical stretching mode of the octahedra. The E_g mode is a doubly degenerate stretching mode affecting oxygen octahedra. The T_{1g} mode (which is not optically active) is triply degenerate and corresponds to tilts of the octahedra. The T_{2g}

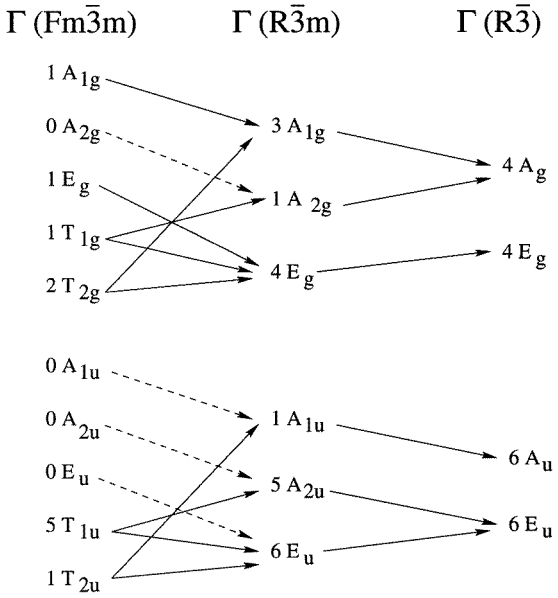

Figure 4. Compatibility relations between the irreducible representation (IR) associated with the vibration modes at the zone centre in the cubic and the trigonal phases of Pb_2MgTeO_6.

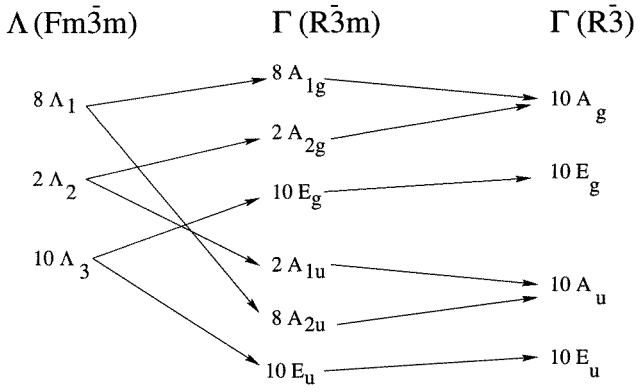

Figure 5. Compatibility relations between the IR associated with the vibration modes at the incommensurate point in the cubic and the trigonal phases of Pb_2MgTeO_6.

modes are triply degenerate and of bending type. It should be noticed that the nonzero elastic strain components measured in the rhombohedral phase belong to the T_{2g} representation. The decomposition also includes *ungerade* modes: one of the five T_{1u} modes has zero frequency, and it represents the zone-centre acoustic modes. Finally, the modes belonging to T_{2u} irreducible representations are not optically active.

Liegeois-Duyckaerts and Tarte (1974) studied the Raman spectra of Pb_2MgTeO_6 and of many other complex perovskites at room temperature. They found that only oxygen atoms can move in A_{1g} and E_g modes. Oxygen atoms vibrate along Te–O–Mg directions, and the frequencies of these modes are mainly affected by the strength of Te–O and Mg–O bonds. Lead atoms are involved in the T_{2g} modes while Te and Mg atoms are always at rest.

Starting from the ideal cubic cell of fully ordered Pb_2MgTeO_6 ($Z = 4$), a symmetry reduction to the trigonal group of the low-temperature cell can be constructed. Two phenomena take place at the phase transition: the onset of the incommensurate superstructure, and the ferroelastic distortion of the lattice. The superstructure appears along only one of the $\langle 111\rangle_c$ directions as shown by the electron microscopy study. The symmetry of the lattice of the low-temperature phase is therefore trigonal.

The point $\boldsymbol{q}_{inc}$ sits on the line Λ which connects the zone centre with the point $L = (\frac{1}{2}\,\frac{1}{2}\,\frac{1}{2})$. The symmetry of the Λ line (and of the point $\boldsymbol{q}_{inc}$) is C_{3v}.

The phase transition towards the incommensurate phase may be associated with the mode condensation occurring at $\pm\boldsymbol{q}_{inc}$. Therefore, we have to analyse the mode symmetries at these points to understand the relationships between these modes in the two phases. The factor group analysis in the cubic phase at $\boldsymbol{q}_{inc}$ gives the following decomposition:

$$\Lambda(\boldsymbol{q}_{inc}) = 8\Lambda_1 \oplus 2\Lambda_2 \oplus 10\Lambda_3$$

in which Λ_3 modes are doubly degenerate.

3.4.2. Compatibility relations. The low-temperature phase is incommensurate, so the tri-periodical translational symmetry is broken.

The comprehension of the phase transition mechanism involves the analysis of the modes that become totally symmetrical in the low-temperature phase. The compatibility relations between the two phases are summarized in figures 4 and 5. We know from a structural resolution at 6 K (Baldinozzi *et al* 1997) that this phase has the four-dimensional space group $R\bar{3}(\delta\delta\delta)$, that the oxygen-modulated displacements are mainly along $\langle 110\rangle_c$, and Mg and Te atoms are not affected by a displacive modulation. In principle, the condensation of any of the modes becoming totally symmetrical in the low-temperature phase can induce this phase transition.

(i) The zone-centre irreducible representation (IR) T_{1g}; this representation corresponds to a rigid tilt of an octahedron.

(ii) The zone-centre modes belonging to the IR T_{2g}; this representation is also involved in the ferroelastic deformation.

(iii) The modes belonging to the IR Λ_1; the modes belonging to this IR result from the vibration of the cations along the threefold axis while the O atoms can vibrate in a quite general way along $\langle 11l\rangle_c$ (see table 2).

(iv) The modes belonging to the IR Λ_2; these modes 'see' the cations at rest while the O atoms vibrate along $\langle 110\rangle_c$.

It may be pointed out that the ferroelastic phase transition $Fm\bar{3}m \rightarrow R\bar{3}(\delta\delta\delta)$ can be described as a two-step mechanism, involving a hypothetical intermediate phase having the space group $R\bar{3}m(\delta\delta\delta)$ (D^5_{3d}), where the modulated displacements of O atoms are much more constrained.

The order parameters of the hypothetical $Fm\bar{3}m \rightarrow R\bar{3}m(\delta\delta\delta)$ phase transition belong to the T_{2g} and Λ_1 IR. In this case, if the primary order parameter belongs to the T_{2g} IR (and, if this one is the elastic strain, the phase transition would be a proper ferroelastic one), it is difficult to explain the appearance of the incommensurate superstructure. For this reason, it is more likely that the primary order parameter belongs to the Λ_1 IR, the elastic strain being a secondary parameter triggered by the first one, so this phase transition would be an improper ferroelastic one. The following phase transition towards the $R\bar{3}(\delta\delta\delta)$ phase would involve the softening of a mode belonging to the Λ_2 IR, and, eventually, of the mode belonging to the T_{1g} IR.

Table 2. Symmetry-adapted eigenvectors of the off-centre zone modes that become totally symmetrical in the trigonal phase $R\bar{3}$.

Atom	Λ_1	Λ_2
Te	α_1	0
	α_1	0
	α_1	0
Mg	β_1	0
	β_1	0
	β_1	0
Pb_1	γ_1	0
	γ_1	0
	γ_1	0
Pb_2	δ_1	0
	δ_1	0
	δ_1	0
O_1	ϵ_1	α_2
	ϵ_1	$-\alpha_2$
	ζ_1	0
O_2	η_1	β_2
	η_1	$-\beta_2$
	θ_1	0
O_3	ζ_1	0
	ϵ_1	α_2
	ϵ_1	$-\alpha_2$
O_4	ϵ_1	$-\alpha_2$
	ζ_1	0
	ϵ_1	α_2
O_5	θ_1	0
	η_1	β_2
	η_1	$-\beta_2$
O_6	η_1	$-\beta_2$
	θ_1	0
	η_1	β_2

On the other hand, if the direct phase transition $Fm\bar{3}m \rightarrow R\bar{3}(\delta\delta\delta)$ occurs directly, it would be induced by a mode belonging to the Λ_2 IR; in this case, modes belonging to the T_{1g} IR, as for the rigid tilt of the octahedron, and the T_{2g} IR, like the elastic deformation, can be triggered in this process.

In the present case, the two-step sequence seems to be the most likely to occur, because this sequence explains the thermal evolution of Raman spectra better (cf. 3.5).

It should be noticed that, up to now, we have limited the mode analysis to centrosymmetrical space groups because we do not possess any evidence for loss of the symmetry centre. If the symmetry centre is lost, the symmetry of the low-temperature phase can be lowered to $R3(\delta\delta\delta)$. The active representation for this phase transformation is A_{2u} which transforms like the spontaneous polarization corresponding to the onset of a dielectric moment along the threefold axis. This polarization would constitute the driving order parameter for this ferroelectric phase, and a coupling via gradient terms to the elastic

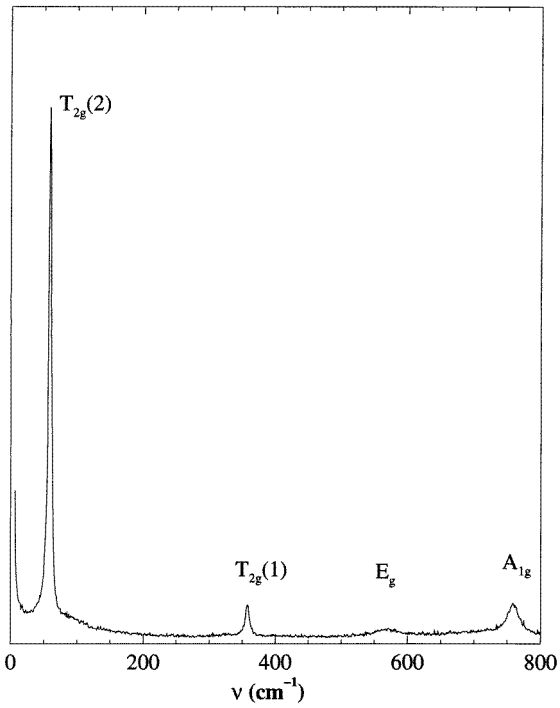

Figure 6. The room temperature Raman spectrum of Pb_2MgTeO_6.

strain would be obvious. As the anomaly of the dielectric permittivity is quite small, this phase transition does not seem to occur.

3.5. Raman scattering

The Raman spectra have been recorded with a Dilor Z24 triple-monochromator instrument equipped for detection with cooled photomultipliers coupled with a counting system. The 514.5 nm emission line of an argon-ion laser (3 W) has been used. The spectral slit widths were typically 2 cm^{-1}. Low-temperature measurements down to 35 K were made using a modified sample holder. The temperature regulation was better than ± 1 K.

A series of Raman spectra from 0 to 1000 cm^{-1} have been collected for a powder sample of Pb_2MgTeO_6 in the low-temperature phase (incommensurate) and in the cubic phase (figure 6). In order to investigate the thermal evolution of the frequencies and widths, the Raman spectra had been carefully fitted, and the accuracy is better than 0.1 cm^{-1}. The spectra were systematically fitted using Lorentzian or Gaussian functions, depending on the profile of the phonon peaks. A classification of the frequencies of the phonon peaks at the lowest temperature, 35 K (figure 7), is given in table 3.

The assignment of the four peaks in the cubic phase is straightforward, owing to the previous work of Liegeois-Duyckaerts and Tarte (1974) and to the group-theoretical predictions. The four frequencies observed in the Raman spectrum at room temperature correspond to A_{1g}, $T_{2g}(1)$, E_g and $T_{2g}(2)$ modes respectively (table 4). It is worth comparing the values of the frequencies and widths of Pb_2MgTeO_6 with the data concerning Pb_2MgWO_6. The frequency of the A_{1g} mode is much lower in the Te compound than in the

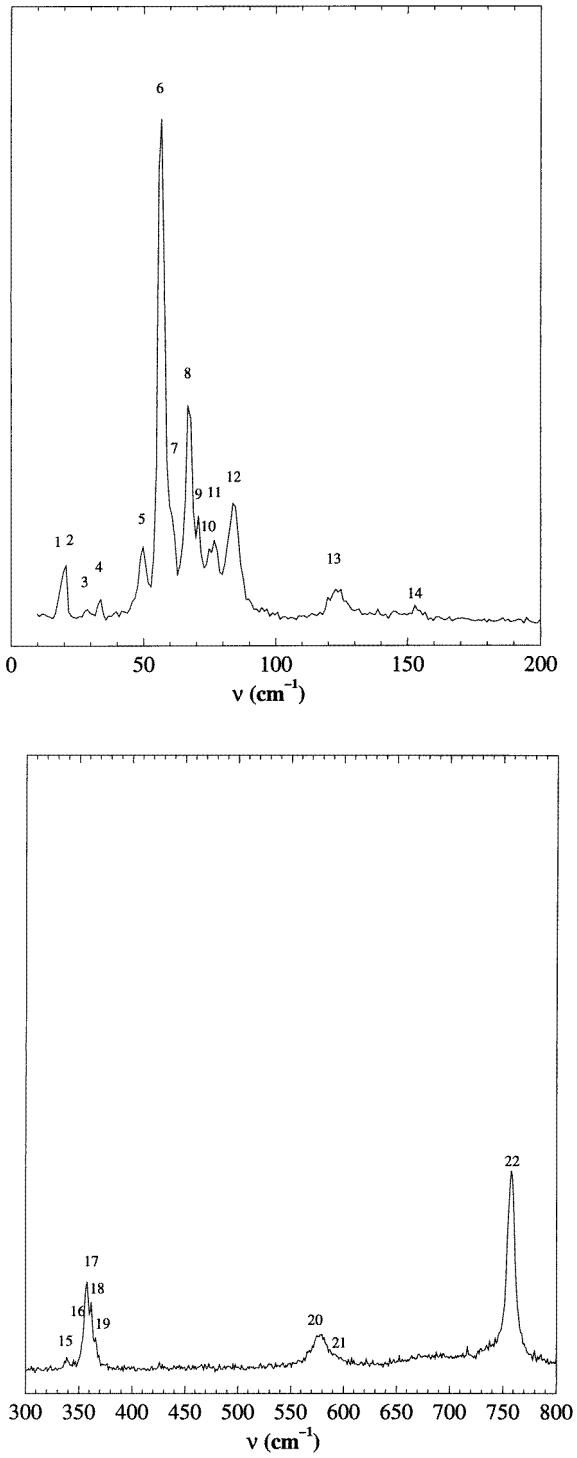

Figure 7. The Raman spectrum of Pb_2MgTeO_6 at 35 K. The frequencies of the lines are reported in table 3.

Table 3. Raman frequencies (cm^{-1}) of Pb_2MgTeO_6 at 35 K.

		$\bar{\nu}$ (cm^{-1})
1		18.4
2		20.3
3		28.3
4		33.4
5		49.8
6	T_{2g}	56.6
7	T_{2g}	60.4
8	T_{2g}	67.2
9		70.8
10		73.6
11		76.9
12		84.0
13		123.8
14		152.3
15		339.9
16	T_{2g}	352.6
17	T_{2g}	357.1
18	T_{2g}	361.5
19		366.1
20	E_g	577.2
21	E_g	592.7
22	A_{1g}	757.8

Table 4. Raman frequencies (cm^{-1}) of Pb_2MgTeO_6 at room temperature and of Pb_2MgWO_6 in the cubic phase just above the phase transition.

$\bar{\nu}$ (cm^{-1})	A_{1g}	E_g	$T_{2g}(1)$	$T_{2g}(2)$	
Pb_2MgTeO_6	759	568	357	58	(This work)
Pb_2MgTeO_6	758	569	357	59	(Liegeois-Duyckaerts and Tarte 1974)
Pb_2MgWO_6	844	—	389	64	(Baldinozzi *et al* 1995)
Pb_2MgWO_6	846	—	389	65	(Kania *et al* 1996)

tungstate. As this mode corresponds to a displacement of O along the Mg–O–Te axis, the result is in agreement with the smaller lattice parameter of Pb_2MgTeO_6. Moreover, Liegeois-Duyckaerts and Tarte (1974) also pointed out the different electronic configurations of Te^{6+} (d^{10}) and W^{6+} (d^0) cations. While the former electronic configuration is unfavourable to the formation of π-bonding between the cation and the O, the d^0 configuration allows the superposition of the t_{2g} orbitals of the metal and of the ligand orbitals, resulting in a strong π-type polarization and increasing the bonding energy. It is also worth noticing that in tungstate compounds the E_g mode is not observed. Finally, the modes of T_{2g} symmetry, where Pb atoms are allowed to vibrate, have a slightly lower frequency in the Te compound.

When the temperature is lowered below the phase transition (about 194 K), the onset of the incommensurately modulated phase induces a loss of the translational periodicity in the crystal. The consequent relaxation of the selection rules allows the existence of phonon frequencies that are otherwise forbidden. For this reason, the Raman spectra in the incommensurate phase are much more complex than those observed in the low-temperature phases of other complex perovskites. Several well resolved sharp peaks are observed in

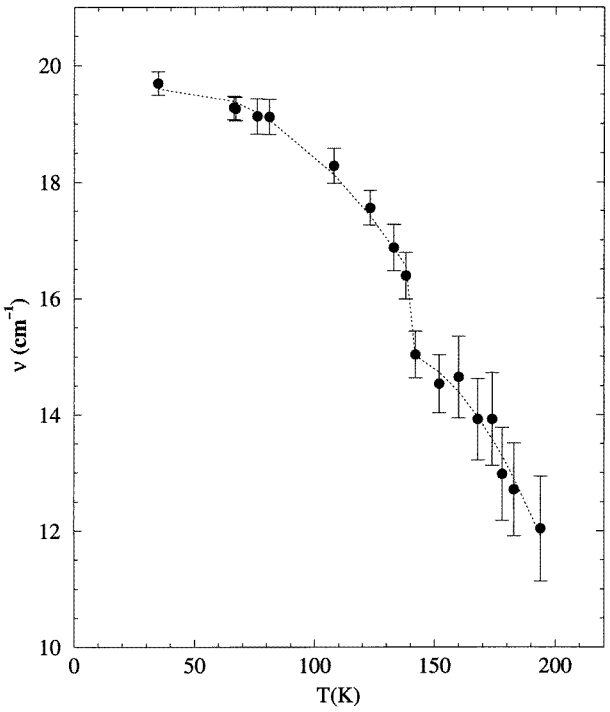

Figure 8. The soft-mode frequency evolution versus T.

the low-frequency part of the spectrum. The analysis of the lower-frequency region of the Raman spectra for the incommensurate phase indicates the existence of a soft mode, condensing at the phase transition. On lowering the temperature below that of the phase transition, the soft mode begins to harden. At the beginning it appears to be strongly overdamped, but the width rapidly decreases on cooling. Small extra signals are observed here and there near the main phonon peaks of the cubic phase, while the main peaks are broadened. This situation evolves abruptly between the spectra at 150 and 142 K:

(i) the soft-mode frequency undergoes a step increase (figure 8);

(ii) the slope of the soft-mode width versus temperature shows a significant decrease (figure 9); and

(iii) the T_{2g} peaks appear to be suddenly split (figure 10).

These distinct features cannot be simply explained by a change of the dynamics of the modulation phase such as the appearance of higher-harmonic terms in the modulation. The coincidence with the incident of the dielectric permittivity seems to support the existence of a structural phase transition at about 142 K. The group-theoretical considerations discussed in the previous section support the hypothesis that the symmetry of the intermediate phase is $R\bar{3}m(\delta\delta\delta)$.

4. Conclusions

The study of the electron microscopy diffraction pattern, of the evolution of the dielectric permittivity with temperature and of the thermal evolution of the Raman spectra allows us

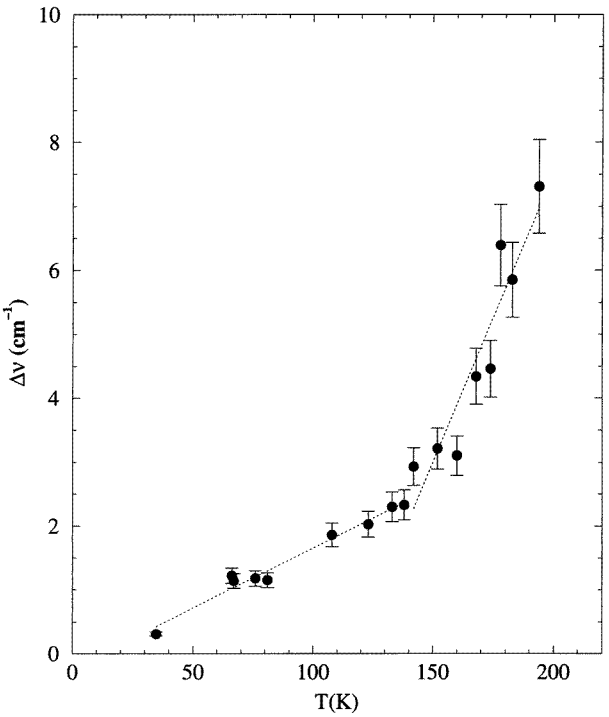

Figure 9. The thermal evolution of the linewidth of the soft mode. A sudden change in the slope is observed at about 142 K.

to point out some characteristic features of the phase transition sequence of Pb_2MgTeO_6.

At about 194 K, the onset of an incommensurately modulated phase of trigonal symmetry is accompanied by the appearance of incommensurate superstructures and by a very small lattice deformation. As was already discussed in a previous paper (Baldinozzi *et al* 1994), the thermal evolution of the ferroelastic trigonal distortion lets us exclude this from consideration as the primary order parameter of the phase transition. The symmetry analysis is in agreement with this result. Therefore, this phase transition is not a proper ferroelastic one, but it is triggered by the condensation of a mode at an incommensurate point of the first Brillouin zone. The analysis of the Raman spectra provides evidence of the existence of such a soft mode, and, starting from the analysis of the compatibility relations of the two phases, the symmetry of this mode has been discussed.

The analysis of the Raman spectra and the existence of a simultaneous incident at about 142 K in the dielectric permittivity measurements constitute evidence of a second phase transition (incommensurate–incommensurate). The structural resolution study at 6 K (Baldinozzi *et al* 1997) allowed us to establish precisely the incommensurate space group of the lowest-temperature phase ($R\bar{3}(\delta\delta\delta)$), but no structural resolution study has been performed for the intermediate incommensurate phase. Therefore, only conjectures can be given as to the symmetry of this intermediate phase. As discussed on the basis of the compatibility relations of the cubic and lowest-temperature phases, the existence of an intermediate phase of symmetry $R\bar{3}m(\delta\delta\delta)$ can be proposed. For this phase, the displacements (static and modulated) of the O atoms are much more constrained, giving a possible explanation for the pseudo-cubic features of the Raman spectra for this phase

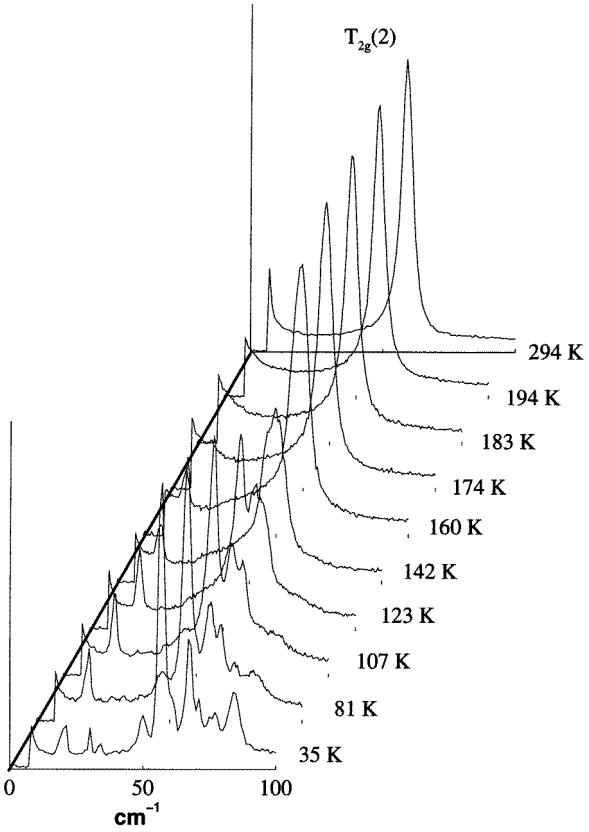

Figure 10. A selection of Raman spectra collected between room temperature and 35 K. The scattered intensity of the T_{2g} line changes suddenly at about 142 K.

(broadening of the main peaks with no apparent splitting). Only in the lowest-temperature phase, where the O atoms show large modulated displacements, do the splitting of the Raman peaks and the appearance of new Raman lines occur.

References

Baldinozzi G, Sciau Ph, Bérar J F and Grebille D 1997 to be published
Baldinozzi G, Sciau Ph and Bulou A 1995 *J. Phys.: Condens. Matter* **7** 8109–17
Baldinozzi G, Sciau Ph, Moret J and Buffat P A 1994 *Solid State Commun.* **89** 441–5
Bayer G 1963 *J. Am. Ceram. Soc.* **46** 604–5
Liegeois-Duyckaerts M and Tarte P 1974 *Spectrochim. Acta* A **30** 1771–86
Kania A, Jahfel E, Kugel G E, Roleder K and Hafid M 1996 *J. Phys.: Condens. Matter* **8** 4441–53
Politova E D and Venevtsev Yu N 1973 *Dokl. Acad. Nauk* **209** 838–41
Randall C A, Markgraf S A, Bhalla A S and Baba-Kishi K 1989 *Phys. Rev.* B **40+41** 413–6
Sciau Ph and Grebille D 1994 *Aperiodic '94; Proc. Int. Conf. on Aperiodic Crystals* (Singapore: World Scientific) pp 460–4
Tamura H 1978 *Ferroelectrics* **21** 449–50
Wilson A J C 1992 *International Tables for Crystallography* vol C (Dordrecht: Kluwer)